Carrier relaxation dynamics and steady-state charge distributions in coupled InGaN/GaN multiple and single quantum wells

S. Khatsevich and D. H. Rich[a)]
Department of Physics, Ilse Katz Center for Meso and Nanoscale Science and Technology, Ben-Gurion University of the Negev, P. O. Box 653, Beer-Sheva 84105, Israel

S. Keller and S. P. DenBaars
Electrical and Computer Engineering and Materials Departments, University of California, Santa Barbara, California 93111

(Received 25 January 2007; accepted 3 March 2007; published online 10 May 2007)

We have examined the carrier capture dynamics and excitation dependent charge distributions of coupled InGaN/GaN multiple quantum well samples. We measured the temporal evolution of time-delayed cathodoluminescence (CL) spectra to study the temperature- and excitation-dependent transfer of carriers from a surrounding confinement region into a coupled single quantum well. Samples possessing two different structures for the confinement region [i.e., number of quantum wells (QWs) and varying widths] were examined with CL. In order to study state filling of the SQW and QWs in the confinement region, we calculated the quasi-Fermi levels and carrier densities by utilizing a model that involves self-consistent solutions of the nonlinear Poisson-Schrödinger equation for wurtzite QWs including strain, deformation potentials, and polarization fields. Band-edge and effective mass parameters were first obtained from a strain- and In composition-dependent $\boldsymbol{k}\cdot\boldsymbol{p}$ calculation for wurtzite $In_xGa_{1-x}N$, using a 6×6 $\boldsymbol{k}\cdot\boldsymbol{p}$ Hamiltonian in the {0001} representation. The model shows that the difference in the quasi-Fermi levels between the confinement and SQW regions decreases with increasing excitation and temperature. Likewise, a reversal in the relative magnitude of the carrier densities between these two regions occurs at a certain temperature and excitation. Furthermore, the results for the model describing the steady-state excitation are consistent with those for the transient excitation in time-resolved CL, which also exhibit a marked increase in the rate of carrier transfer to the SQW region as the temperature increases. © *2007 American Institute of Physics*. [DOI: 10.1063/1.2727437]

I. INTRODUCTION

Intense research in the optical and structural properties of InGaN/GaN quantum wells (QWs) and heterostructures has led to the remarkable developments of green, blue, and violet laser diodes in the past decade which are now commercially available for applications in lighting, display, and optical storage devices.[1] Notwithstanding the success story, many questions still remain regarding stoichiometric fluctuations in ternary InGaN thin films that lead to sub-micron fluctuations in the alloy composition[2–7] and attendant variations in fields induced by piezoelectric and spontaneous polarizations.[8–11] In particular, the band profiles in coupled InGaN QW systems will be affected by alloy fluctuations and strain relaxation that will affect the details of the microscopic polarization in both the QWs and adjacent barriers. Many studies have reported the important role of the large internal electric field in InGaN QWs,[10] comparable to or much larger than ~1 MV/cm, which induces a large red-shift in the transition energies,[12,13] due to the quantum confined Stark shift effect (QCSE),[13–15] and attendant reduction in the oscillator strength,[13,15,16] owing to the field-induced separation of the electron and hole wave functions toward the opposite sides of the QW. An improved understanding of the optical properties of InGaN/GaN MQWs at various temperatures and levels of excitation is of particular importance for the optimal design of InGaN/GaN light-emitting devices. In order to increase the efficiency of carrier collection and luminescence in such quantum systems, issues still remain regarding on how to best tailor the region surrounding the QW, which we refer to as the confinement region (CR).

In this paper, we examine the carrier relaxation dynamics and band filling of coupled InGaN/GaN SQW samples possessing different QW structures in the CR. The QWs in the CR are designed to allow for electronic coupling to the SQW, which possesses lower energy levels relative to those in the CR. From a fundamental perspective, it would be useful to construct a detailed experimental and theoretical analysis of selectively positioned InGaN QWs in the CR adjacent to a typical optically active InGaN SQW such that carrier transfer between the regions occurs by diffusive transport and electronic coupling. In this way, the carrier relaxation and transfer dynamics to the lower energy SQW can be studied by time-delayed CL spectra, which reflect snapshots of the carrier transfer and recombination processes. In order to study state filling of the SQW and QWs in the confinement region, we calculate the quasi-Fermi levels and carrier densities by utilizing a model that involves self-consistent solutions of the nonlinear Poisson-Schrödinger equation for wurtzite QWs including strain, deformation potentials, and polarization fields. Band-edge and effective mass parameters

[a)]Electronic mail: danrich@bgu.ac.il

 © 2007 American Institute of Physics

Downloaded 11 May 2007 to 132.72.138.1. Redistribution subject to AIP license or copyright, see http://jap.aip.org/jap/copyright.jsp

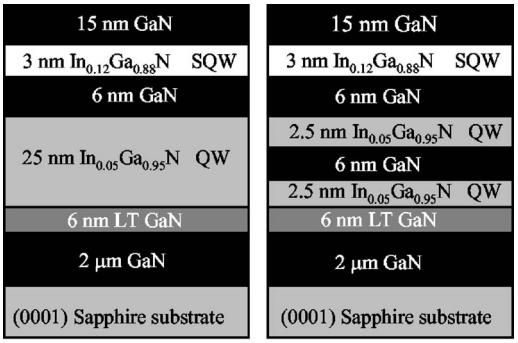

FIG. 1. Schematic diagram of the structure for our coupled InGaN/GaN QW samples showing the CR and SQW regions. The SQW region for both samples S1 and S2 contains a single nominal $In_{0.12}Ga_{0.88}N$ QW. The thicknesses for the regions shown in the diagrams are not to scale.

were first obtained from a strain- and In composition-dependent $\boldsymbol{k}\cdot\boldsymbol{p}$ calculation for wurtzite $In_xGa_{1-x}N$, using a 6×6 $\boldsymbol{k}\cdot\boldsymbol{p}$ Hamiltonian in the {0001} representation. We have used this model in conjunction with CL under various steady-state excitations to better understand the carrier transfer from the CR to the SQW in terms of variations in the calculated quasi-Fermi levels and charge distributions in both regions.

II. EXPERIMENTAL DETAILS

The InGaN MQW samples were grown on *c* plane sapphire by metal organic chemical vapor deposition (MOCVD) using trimethylgallium, trimethylindium, disilane, and ammonia as precursors, which has been described previously.[17] Two InGaN MQW samples were examined in this study. First, a 2 μm-thick GaN:Si buffer layer was grown on a *c* plane sapphire substrate at 1060 °C, followed by a deposition of a 6 nm low temperature (LT) GaN layer. The confinement region (CR), the 3 nm-thick $In_xGa_{1-x}N$ SQW with $x=0.12$, nominally, and the 15 nm-thick GaN capping layer were grown at 800 °C. In sample S1, a 25 nm-thick $In_yGa_{1-y}N$/6 nm-thick GaN confinement layer with low nominal indium composition $y\approx0.05$ was deposited in the confinement region prior to growth of the $In_{0.12}Ga_{0.88}N$ SQW. In the other sample (labeled as S2) two periods of a 2.5 nm-thick $In_{0.05}Ga_{0.95}N$/6 nm-thick GaN layer were deposited prior to the SQW. Schematic illustrations of the two sample structures are shown in Fig. 1.

The cathodoluminescence (CL) experiments were performed with a modified JEOL-5910 scanning electron microscope (SEM) using a 15 keV electron beam with probe current in the range of 0.03–40 nA.[18] A UV multialkali photomultiplier tube (PMT) operating in the 185–850 nm spectral range enabled the photon counting of the luminescence that was dispersed by a 0.25 m monochromator. Measurements were performed at different temperatures in the 50–310 K temperature range. In order to increase the range of accessible excitation densities, the excitation volume was varied by defocusing the electron beam in reproducible steps as has been described in detail elsewhere.[19,20] In the very low excitation density regime, the electron beam was defocused to a spot with a diameter of ~90 μm at the sample surface. The defocusing approach permits measuring CL emission with a uniform excitation density that is several orders of magnitude smaller than what can be employed using a focused electron beam.[20] The relationship between the excitation density, P, and probe current, I_b, can be approximated by

$$P \approx \frac{I_b E_b}{e S_e}, \tag{1}$$

where E_b is the e-beam energy (15 keV), and S_e is the excitation area, which is 3 and 6300 μm^2 for focused and defocused electron beams, respectively. For $I_b=400$ pA, this yields an excitation density of 200 W/cm^2 and 95 mW/cm^2 for focused and strongly defocused e-beams, respectively. Time-resolved CL experiments were performed with the method of delayed coincidence in an inverted single-photon counting mode, with a maximum time resolution of ~100 ps.[18,21] Electron beam pulses of 50 ns width with a 1 MHz repetition rate were used to excite the sample. Steady-state and time-delayed CL spectra were acquired with a spectral resolution of 1 nm.

III. RESULTS AND DISCUSSION

A. Time-resolved CL spectroscopy

In order to examine the relaxation and collection of carriers into the SQW time-delayed CL spectra were obtained for samples S1 and S2 at temperatures in the $50\leq T\leq310$ K range. Figures 2 and 3 show time-delayed CL spectra for samples S1 and S2, respectively, at temperatures of 50 and 260 K. All spectra are renormalized to have about the same maximum peak height. The time windows O1–O10 and D1–D12 denote time windows relative to the beginning of onset and decay, respectively, of the luminescence, as referred to the beginning and end of the electron beam pulses. The constant excitation spectra, which were measured in the center of the 50 ns excitation pulse, are labeled *In Pulse* in Figs. 2 and 3. These spectra are essentially identical to the CL spectra obtained from CL acquired under constant excitation conditions with an excitation density $P=200$ W/cm^2.

At high temperatures, emission for the constant excitation spectra is dominated by the SQW luminescence, as seen in the spectra labeled as *In Pulse* in Figs. 2 and 3. This is consistent with previous results for samples possessing similar structures.[17] At low temperatures both samples emit predominately from the confinement region, with a much weaker emission that stems from the SQW. For an e-beam energy of 15 keV, about 95% of the electron-hole pairs are created deep in the GaN buffer layer, below the confinement region. It is, therefore, natural to assume that the initial carrier capture from the GaN buffer layer into the CR is followed by carrier transfer from the CR into the SQW. In Fig. 4, we plot the ratio of the integrated intensities of the SQW and the CR, I_{SQW}/I_{CR}, versus temperature to illustrate the thermally activated nature of the carrier transfer from the QWs of the CR into the SQW for both samples. Previously, we have calculated activation energies related to such a carrier transfer.[22] Also shown in Fig. 4 are the ratios I_{SQW}/I_{CR}

Downloaded 11 May 2007 to 132.72.138.1. Redistribution subject to AIP license or copyright, see http://jap.aip.org/jap/copyright.jsp

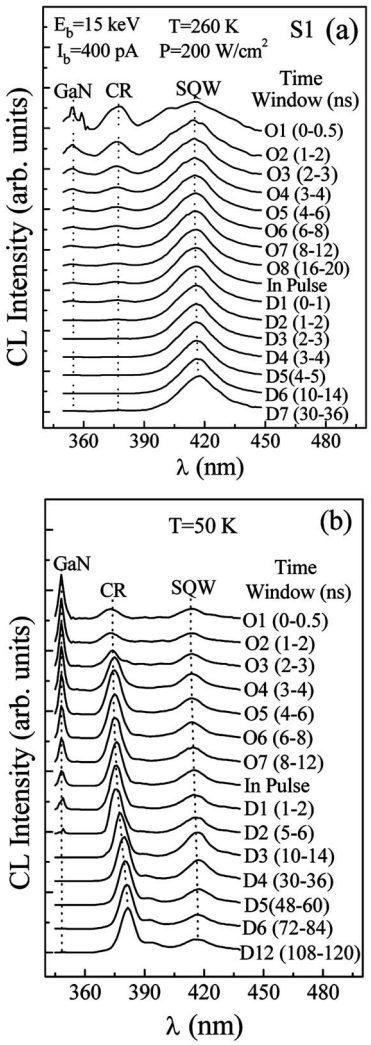

FIG. 2. Time-delayed CL spectra acquired for sample S1 at temperatures (a) $T=260$ K and (b) $T=50$ K for the case of high excitation density, $P=200$ W/cm^2. The spectra are shown for various onset (Oi) and decay (Di) time windows. All spectra are normalized to have about the same maximum peak height. The SQW and the CR peak positions at different time windows are indicated by vertical dashed lines. A strong red-shift of the CR emission is seen in the decay windows at 50 K.

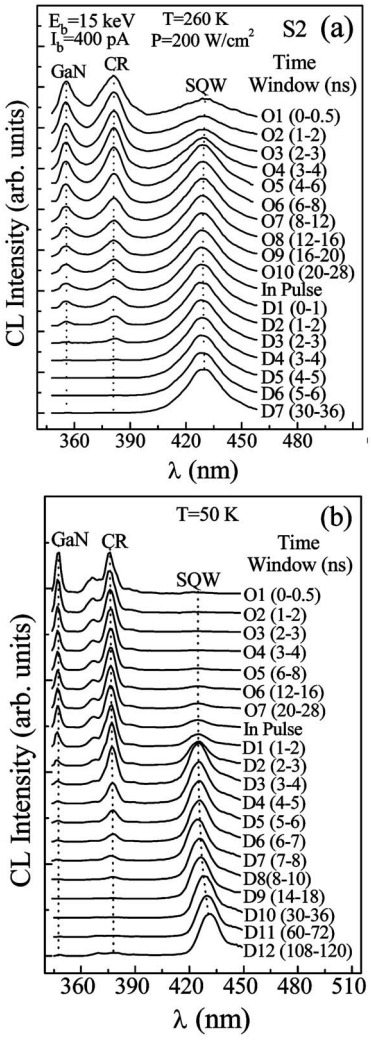

FIG. 3. Time-delayed CL spectra acquired for sample S2 at temperatures (a) $T=260$ K and (b) $T=50$ K for the case of high excitation density, $P=200$ W/cm^2. The spectra are shown for various onset (Oi) and decay (Di) time windows. All spectra are normalized to have about the same maximum peak height. The SQW and the CR peak positions at different time windows are indicated by vertical dashed lines. A strong red-shift of the SQW emission is seen in the decay windows at 50 K.

for the cases of a high and low excitation density (200 W/cm^2 and 95 mW/cm^2, respectively). It is apparent that a marked enhancement of the relative carrier transfer from the CR to the SQW occurs at high excitation densities. This can be explained by (i) band filling of the QWs of the CR at higher excitation densities, which will facilitate a thermally enhanced escape of carriers from the QWs of the CR and (ii) a saturation of nonradiative recombination channels in the SQW as the excitation density is increased. The band filling of the QWs of the CR and attendant changes in the quasi-Fermi levels that favor carrier transfer from the CR to SQW will be presented in the model discussed in Sec. III B. The saturation of nonradiative channels has been demonstrated by considering the excitation dependence of the decay lifetime for similar samples.[22] These previous results showed that the nonradiative lifetime, τ_{NR}, has an excitation dependence in which τ_{NR} increases with the excitation density at high temperatures.[22]

In the time-delayed spectra of Figs. 2 and 3, the initial rise of the GaN peak indicates that most of the electron-hole pairs are created deep in the GaN buffer layer, below the CR, due to the large e-beam energy of 15 keV. The rapid rise of the CR peak at the shortest time window O1 (centered at 250 ps) reflects the rapid capture of carriers into QWs of the confinement region from the GaN buffer layer. For sample S2 at low temperatures, the initial rapid rise of the GaN and the CR peaks is followed by a relatively slow rise of the SQW peak with peak intensity close to zero at the shortest onset (Oi) time windows, as seen in Fig. 3(b). The increase in CL intensity of the SQW peak is well correlated with a relative decrease in CL intensities of the GaN and CR peaks in the decay (Di) windows and is attributed to the carrier transfer from QWs of the CR into the SQW. At higher temperatures (~260 K), a much more rapid rise of the SQW peak in the onset time windows corresponds to a more efficient carrier transfer from the CR into the SQW, as is seen

Downloaded 11 May 2007 to 132.72.138.1. Redistribution subject to AIP license or copyright, see http://jap.aip.org/jap/copyright.jsp

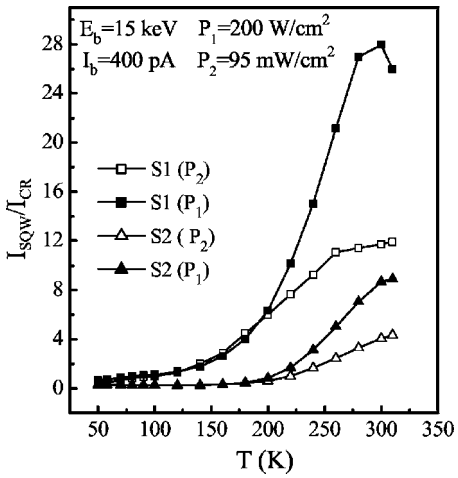

FIG. 4. The ratio of the integrated CL intensities of the SQW and the CR, I_{SQW}/I_{CR}, vs temperature. The graph illustrates the thermally activated nature of the carrier transfer from the QWs of the CR into the SQW for both samples S1 and S2.

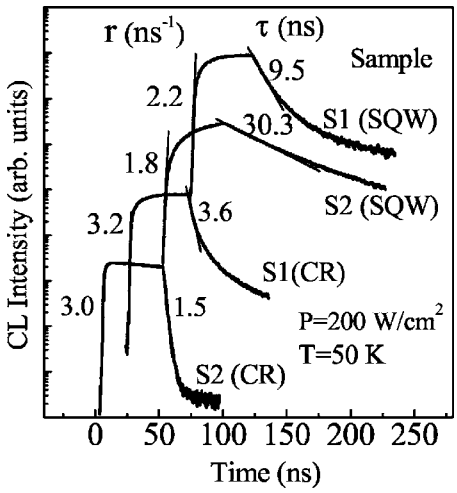

FIG. 5. CL transients (intensity vs time) of the CR and SQW peak emissions. The transients show the onset and decay of the CR and SQW peak luminescence for samples S1 and S2, as labeled. The transients were acquired under high excitation density, $P=200\ \mathrm{W/cm^2}$ at $T=50$ K. Initial onset rates r and decay times τ, obtained by a linear fit from the slopes of the onset and decay curves, are indicated for each sample.

for both samples in Figs. 2(a) and 3(a). In contrast to sample S2, sample S1 shows a rapid rise of the SQW peak even at low temperatures, as seen in Fig. 2(b), most likely due to a more efficient carrier transfer into the SQW.

During the decay stage of the luminescence, narrowing and red-shifting of both the CR and SQW emissions are observed at low temperatures, as seen in Figs. 2(b) and 3(b). The strongest red-shift in the CR peak position of ~80 meV was observed for sample S1 in Fig. 2(b), consistent with the presence of the single 25 nm-thick QW in the confinement region. It is well accepted that InGaN QW systems have large internal electric fields that induce a large red-shift in the transition energies, resulting from the QCSE. This effect is consequently more pronounced for thicker QWs.[13] For spectra acquired under steady-state and approximately constant excitation conditions (labeled as *In Pulse* in Figs. 2 and 3), the carrier density in the QWs under high excitation can be sufficient to partially screen the internal field.[23–26] During the decay stage of the luminescence, the screening of the field decreases due to the loss of excess carriers by various decay processes and carrier spectral diffusion into lower-energy states.[27] The increase in the internal electric field leads to a red-shifting of the QW emission, as seen in Figs. 2(b) and 3(b). At higher temperatures, the CR emission in all samples decays rapidly in the time windows D1–D4, owing to nonradiative processes and a high transfer and quantum capture rate into the SQW, as seen in Figs. 2(a) and 3(a).

In order to further study the temporal behavior, the initial onset and decay curves of the CR and SQW peak emissions were measured at different temperatures and excitations. To quantify the initial increase in the CL intensity with time, the onset rate, which is defined as $r=\Delta\ln(I_{CL})/\Delta t$, is given by the slopes of the tangents to the onset curves for the semilog plots of the CL transients in Fig. 5. The initial onset rates measured at $T=50$ K and high excitation, $P=200\ \mathrm{W/cm^2}$, for sample S2 are 1.8 and 3.0 $\mathrm{ns^{-1}}$ for the SQW and CR emissions, respectively, as shown in Fig. 5. The results reveal that the onset rates of the CR emission with $r\approx 3\ \mathrm{ns^{-1}}$ are considerably greater than that of the SQW emission with $r\leq \sim 2\ \mathrm{ns^{-1}}$. This further supports the notion of fast carrier capture into the CR region from the GaN buffer layer followed by a slow carrier transfer through or over the barriers into the SQW. This behavior is responsible for the slow rise of the SQW peak at low temperatures, as observed in the time-delayed spectra. The larger initial onset rates of the CR and SQW emissions were found for sample S1 (as shown in Fig. 5), consistent with the existence of a single QW in the CR for this sample. Likewise, the initial luminescence decay times τ are measured from the slopes in the decay part of the $\ln(I_{CL})$ versus time transients of the CR and SQW peaks, as indicated in Fig. 5. The initial decay lifetimes of the SQW peak emission measured at $T=50$ K and high excitation are 9.5 and 30.3 ns for samples S1 and S2, respectively. Such differences in decay times were previously attributed to differences in the polarization field between samples possessing otherwise similar QW widths and In compositions.[22] Significantly shorter decay lifetimes of the CR peak luminescence measured at $T=50$ K indicate that carrier transfer into the SQW is efficient even at low temperatures.

The presence of slower decay components in the CL transients of Fig. 5 is a result of a partial screening of the polarization field in the QWs during the initial part of the decay.[22–26] As the carrier density decreases during the decay, the screening of the field is reduced, leading to a longer decay time for carriers remaining. Such screening was found to occur in a variety of similar InGaN/GaN QW structures under high excitation at low temperatures.[22] The slower components near the rising edge of the CL transients for the SQWs of both samples, as observed in Fig. 5, reflect an accumulation of carriers that are initially captured in the CR and subsequently tunnel to the SQW. For temperatures greater than ~100 K, a combination of tunneling and thermal re-emission occurs during the transfer of carriers from the QWs of the CR to the SQW.[22]

Downloaded 11 May 2007 to 132.72.138.1. Redistribution subject to AIP license or copyright, see http://jap.aip.org/jap/copyright.jsp

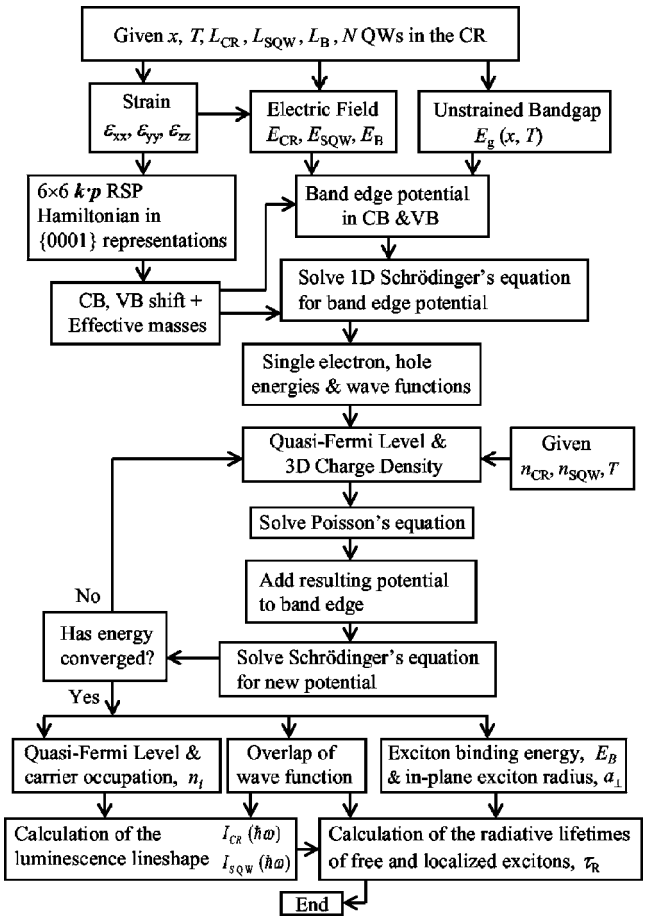

FIG. 6. Flow chart illustrating the details of the model calculations of the excitation dependent eigenstates and quasi-Fermi levels for the coupled InGaN/GaN QW structures of S1 and S2. The model involves self-consistent solutions of the nonlinear Poisson-Schrödinger equation for wurtzite QWs including strain, deformation potentials, and polarization fields.

B. Calculations of eigenstates, quasi-Fermi levels, and carrier densities

In order to model our luminescence data theoretically, to determine values of electric field in the QWs of the CR and SQW, and to model nonlinear effects associated with carrier capture from the CR into the SQW, we solved self-consistently the Schrödinger and Poisson equations, within a single band effective mass approximation. By doing so, we calculate the electron and hole wave functions and energy levels while taking into account the modifications of the potential profile caused by the accumulation of carriers in QWs of the CR and SQW. We have previously described some of the details of this modeling in Ref. 22. We also illustrate our modeling procedure with a flow chart in Fig. 6. Band-edge and effective mass parameters were first obtained from a strain- and In composition-dependent $\boldsymbol{k}\cdot\boldsymbol{p}$ calculation for wurtzite $In_xGa_{1-x}N$, using a 6×6 $\boldsymbol{k}\cdot\boldsymbol{p}$ Hamiltonian in the {0001} representation.[28] The relevant parameters in the $\boldsymbol{k}\cdot\boldsymbol{p}$ method for a wurtzite crystal include the A_i, which are similar to the Luttinger parameters in a zinc-blende crystal; the D_i, which are the deformation potentials for the $In_xGa_{1-x}N$ layers; c_{ij}, the elastic constants; and ε_{ij}, the strain tensor elements.[28] The $\boldsymbol{k}\cdot\boldsymbol{p}$ parameters for $In_xGa_{1-x}N$ were obtained by linearizing between those for InN and GaN for a given composition x. The strain tensor components, ε_{ij}, along with the piezoelectric tensor elements, d_{ijk}, and spontaneous polarization parameter, P_{sp}, are also used to calculate the polarization of the well (barrier) material along the (0001) axis.[29] All numerical parameters that were employed in our $\boldsymbol{k}\cdot\boldsymbol{p}$ and polarization calculations are available elsewhere.[30] We show a flow chart in Fig. 6 describing the procedure and order of our self-consistent approach for solving the nonlinear Poisson-Schrödinger equation. The calculations for the coupled MQW-SQW system include the effects of strain, deformation potentials, and piezo-electric field to obtain the excitation-dependent eigenstates, quasi-Fermi levels, and carrier densities.

After a determination of the valence band energy dispersions for a given In composition, the heavy- and light-hole effective masses for dispersion along ⟨0001⟩, m_{hh}^z and m_{lh}^z, and the average in-plane effective masses, m_{hh}^{xy} and m_{lh}^{xy}, were determined. Our calculations yield $m_{hh}^z=(1.1+0.327x+0.231x^2)m_o$ and $m_{lh}^z=(1.099+0.339x+0.222x^2)m_o$ for $0<x<1$ and $m_{hh}^{xy}=(1.628+0.022x-0.132x^2)m_o$ and $m_{lh}^{xy}=(0.267-0.082x)m_o$ for $x<0.2$. The electron effective masses for dispersion in the QW $x-y$ plane and along the QW z direction are obtained by a linearization between values for InN and GaN as $m_e^{xy}=(0.23-0.13)m_o$ and $m_e^z=(0.19-0.08)m_o$.[30] The conduction to valence band offset in wurtzite $In_xGa_{1-x}N$ is assumed to be independent of x, and is taken as $\Delta E_c/\Delta E_v=70/30$, as has been proposed recently by different researchers.[30–32] We take the unstrained $In_xGa_{1-x}N$ bandgap at an arbitrary temperature as[33,34]

$$E_g^{In_xGa_{1-x}N}(T)=E_g^{In_xGa_{1-x}N}(0)-\frac{10^{-3}T^2}{(1196+T)},$$
$$E_g^{In_xGa_{1-x}N}(0)=0.7x+3.5(1-x)-2.72x(1-x), \tag{2}$$

where $E_g^{In_xGa_{1-x}N}(0)$ is the unstrained $In_xGa_{1-x}N$ bandgap at $T=0$ K.[34] The strain-induced increase in the bandgap is given by solutions from the $\boldsymbol{k}\cdot\boldsymbol{p}$ calculations which included the deformation potentials for a particular strain tensor.[30]

To construct an initial potential profile we used the following assumptions: (i) The potential energies on the far right and far left of the MQW structure are the same[35,36] and (ii) the potential drop over the confinement region is independent of that over the SQW and capping layer and is equal to zero. The second assumption (ii) allows for a decoupling of the CR and SQW regions and enables the determination of the internal electric field in the QWs for these regions independently. From (i) and (ii) with an additional assumption that the electric displacement is conserved along the growth axis,[35,37] we obtain

$$E_W^{CR}=-\frac{E_BL_B}{L_W^{CR}}=\frac{L_B(P_B-P_W^{CR})}{(\varepsilon_W^{CR}L_B+\varepsilon_BL_W^{CR})},$$
$$E_W^{SQW}=-\frac{E_CL_C}{L_W^{SQW}}=\frac{L_C(P_B-P_W^{SQW})}{(\varepsilon_W^{SQW}L_C+\varepsilon_BL_W^{SQW})}, \tag{3}$$

where L_W, L_B, and L_C are the well, barrier, and capping layer widths, respectively, ε_W (ε_B) is the well (barrier) static di-

Downloaded 11 May 2007 to 132.72.138.1. Redistribution subject to AIP license or copyright, see http://jap.aip.org/jap/copyright.jsp

electric constant, E_W (E_B/E_C) is the electric field in the well (barrier/capping layer), and P_W (P_B) is the polarization of the well (barrier) material, which includes both the piezoelectric and spontaneous polarizations. Superscripts denote the SQW and CR regions, respectively. Using Eq. (3), we estimate values of the electric field in the QWs of the CR with 5% In composition as 0.15 and 0.54 MV/cm for samples S1 and S2, respectively. For the SQW with a 12% In composition, the estimated value of the electric field is ~1.57 MV/cm. We have previously shown that a refinement of these fields is possible by considering the temperature dependence of the radiative lifetime of the SQW emission, changes in the actual In composition x in comparison to the nominal compositions attempted during growth, and screening of the fields in the CR regions as a function of excitation density.[22] Rather than focus on refinements in In composition and field, we will focus here on the calculated temperature- and excitation-dependent behavior of the electron and hole quasi-Fermi levels in the CR and SQW regions.

The energy levels and single-particle electron and hole wave functions, $\psi_{e,h}(z)$, were determined by slicing the structures into thin layers and using a finite-element technique, modified for the case of variable effective masses, to find solutions to the Schrödinger equation for a particle subject to an electric field.[24,26,38,39] For a given excess carrier concentration n, using the two-dimensional density of states which is proportional to the appropriate in-plane effective masses, we calculate the population of each quantized state and the quasi-Fermi levels for electrons and holes. The electron and heavy- light-hole carrier densities, n_i^e and $n_j^{hh,lh}$, in these quantized states can be determined by integrating the product of the 2D density of states and the Fermi-Dirac function. The quasi-Fermi levels, $\phi_{e,h}$, are determined by solutions of the following equations:

$$n_i^e = \frac{4\pi m_e^{xy}}{h^2}\left\{kT\ln\left[1+\exp\left(\frac{E_i^e-\phi_e}{kT}\right)\right]-E_i^e+\phi_e\right\},$$

$$n_j^{hh,lh} = \frac{4\pi m_{hh,lh}^{xy}}{h^2}\left\{kT\ln\left[1+\exp\left(\frac{\phi_h-E_j^{hh,lh}}{kT}\right)\right]-\phi_h+E_j^{hh,lh}\right\}, \tag{4}$$

$$n=\sum_{i=1}^{S_e} n_i^e=\sum_{j=1}^{S_{hh}} n_j^{hh}+\sum_{j=1}^{S_{lh}} n_j^{lh},$$

where S_e, S_{hh}, and S_{lh} give the number of energy states considered in the calculations for electrons, heavy holes, and light holes, respectively. In this calculation all bound states were included, and resulted in 17 electron and 32 heavy- and light-hole states as calculated for sample S1. The spectrum of energy states associated with the single-electron and hole wave functions, as computed numerically, can be separated according to their localization in QWs of the CR and SQW. Using these eigenvalues, quasi-Fermi energies for electrons and holes in the CR and SQW were separately determined for a given steady-state carrier density using Eq. (4).

Given the population of each quantized level, we calculate the modification of the potential by solving Poisson's equation

$$\frac{d^2V}{dz^2}=-\frac{[\rho_e(z)+\rho_{hh}(z)+\rho_{lh}(z)]}{\varepsilon\varepsilon_0}, \tag{5}$$

where the average three-dimensional charge densities of electrons, heavy holes, and light holes, $\rho_e(z)$, $\rho_{hh}(z)$, and $\rho_{lh}(z)$, are given by

$$\rho_e(z)=-e\sum_{i=1}^{S_e} n_i^e|\psi_i^e(z)|^2,$$

$$\rho_{hh}(z)=e\sum_{j=1}^{S_{hh}} n_j^{hh}|\psi_j^{hh}(z)|^2, \tag{6}$$

$$\rho_{lh}(z)=e\sum_{j=1}^{S_{lh}} n_j^{lh}|\psi_j^{lh}(z)|^2.$$

The total three-dimensional charge densities of electrons and holes at any arbitrary position along the MQW growth direction z are obtained by summing the charge densities calculated for the CR and SQW. The technique that was employed to solve Poisson's equation subject to the Dirichlet boundary conditions, $V(z)\to 0$ as $z\to\pm\infty$, is a Fourier-series expansion of the potential and three-dimensional charge density.[40]

The exciton binding energies E_B in QWs of the CR and SQW were determined by substitution of respective single-electron and hole wave functions, computed numerically using a finite-element technique, into a radial eigenvalue equation that involves the electron-hole relative motion in an effective in-plane Coulomb potential.[30,41] We used the method of finite differences to solve the eigenvalue equation for E_B. The calculated exciton binding energies in samples S1 and S2 are 2 and 5 meV, respectively, for the CR and are approximately 26 meV for the SQW. It was previously established that the exciton binding energy approaches zero for temperatures $T\geqslant E_B/k_B$ and for carrier densities on the order of $\sim 10^{11}$ cm^{-2}.[42] Such densities are easily accessible in QWs of the CR for the high excitation densities used in this study.

The calculated self-consistent potential profile together with the electron and heavy-hole energies, quasi-Fermi energy levels, probability densities for the electrons and holes, $\psi_{e,h}^*(z)\psi_{e,h}(z)$, for the various labeled states and charge densities are shown in Figs. 7 and 8, respectively, for samples S1 and S2 at $T=58$ K and $P=200$ W/cm^2. In order to facilitate comparisons between the valence- and conduction-band potential profiles and different charge-density functions, the valence-band potential is shown inverted. A large potential drop between the confinement region and the SQW, owing to the difference in quasi-Fermi energies, as seen in Figs. 7 and 8, further justifies the observed efficient carrier transfer from QWs of the CR into the SQW for this excitation density. At low and intermediate temperatures, when emission from the confinement region dominates in the spectra, as seen from Figs. 2(b) and 3(b), the relationship between the steady-state carrier density n_{CR} in the confinement region and the excitation density P can be approximated by

Downloaded 11 May 2007 to 132.72.138.1. Redistribution subject to AIP license or copyright, see http://jap.aip.org/jap/copyright.jsp

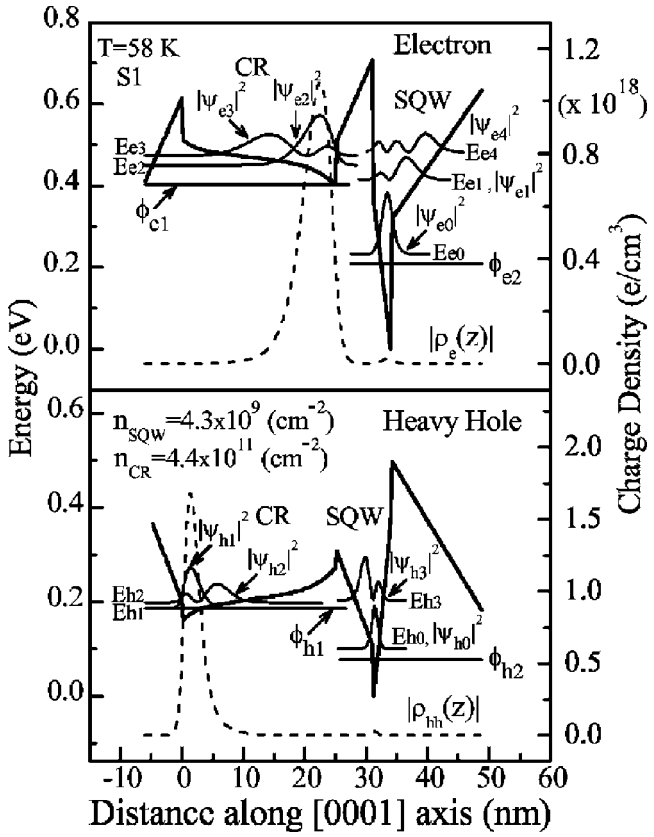

FIG. 7. The self-consistent calculation of the electron and hole potential profiles for the structure of sample S1 at $T=58$ K and high excitation density, $P=200$ W/cm^2. The carrier densities in the CR and SQW, determined by model calculations, are indicated. Valence- and conduction-band potential profiles are shown by thick solid lines. Electron and heavy-hole energies, probability densities for the electrons and holes, $\psi^*_{e,h}(z)\psi_{e,h}(z)$, for the various labeled states, and quasi-Fermi energies are shown by thin solid lines. The electron and heavy-hole charge-density functions, $\rho_e(z)$ and $\rho_{hh}(z)$, respectively, are shown by dashed lines. In order to facilitate comparisons between the valence- and conduction-band potential profiles and different charge-density functions, the valence-band potential is shown inverted.

$$n_{\mathrm{CR}} \approx \frac{P\tau_{\mathrm{QW}}}{3E_g}, \tag{7}$$

where E_g is the bandgap of GaN, and τ_{QW} is the carrier lifetime in QWs of the CR. We estimated the steady-state carrier sheet densities, n_{CR}, in the confinement region at $T=58$ K and $P=200$ W/cm^2 as 4.4×10^{11} and 1.8×10^{11} for samples S1 and S2, respectively. Carrier densities in the CR and SQW at larger temperatures were then determined by comparison of simulated and experimental CL spectra, as described in Ref. 22.

From the model, we calculated the quasi-Fermi levels and carrier densities in the CR and SQW as a function of temperature for the high and low excitation densities, as shown for sample S2 in Fig. 9. In Fig. 9(a), the differences in electron and hole quasi-Fermi levels between the CR and SQW regions, $\Delta\phi_e=\phi_{e1}-\phi_{e2}$ and $\Delta\phi_h=\phi_{h1}-\phi_{h2}$, are shown versus temperature. As the temperature increases, these calculations show that $\Delta\phi_e$ and $\Delta\phi_h$ decrease in magnitude, indicative of an increased equilibration of the carrier densities between the CR and SQW regions. Thus, from the determination of the quasi-Fermi levels, steady excitation is expected to result in an enhanced carrier transfer to the SQW as the temperature is increased, consistent with the results of the CL intensity ratios of Fig. 4 for steady-state excitation. Furthermore, as the excitation density is increased from 95 mW/cm^2 to 200 W/cm^2, $\Delta\phi_e$ and $\Delta\phi_h$ decrease at a faster rate with temperature, consistent with the expectation that band filling in the CR should lead to an enhanced carrier equilibration between the CR and SQW regions.

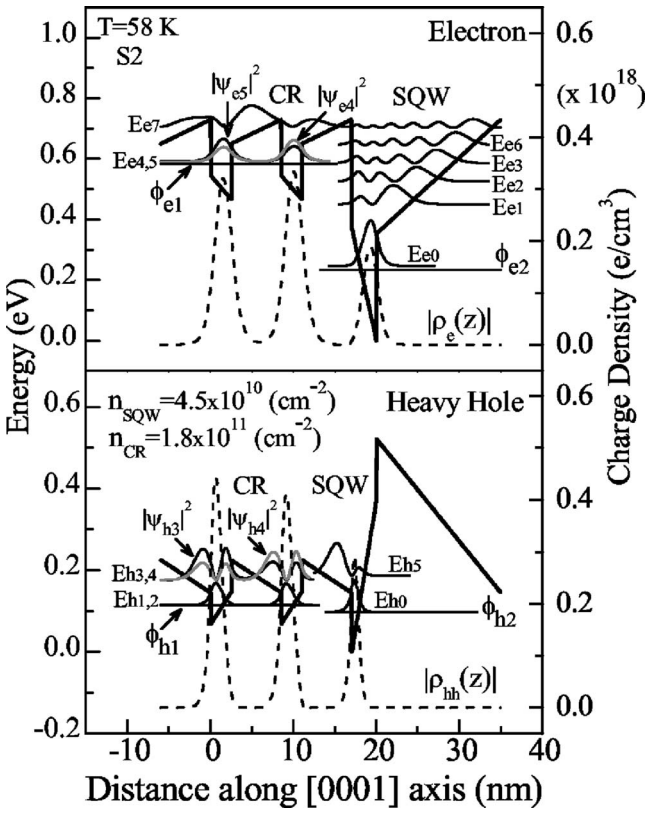

FIG. 8. The self-consistent calculation of the electron and hole potential profiles for the structure of sample S2 at $T=58$ K and high excitation density, $P=200$ W/cm^2. The caption of Fig. 7 also provides a description of the additional features.

These results are further confirmed by a comparison with the temperature dependence of the carrier densities in the CR and SQW regions (n_{CR} and n_{SQW}, respectively), as shown in Fig. 9(b). The results demonstrate that an inversion of the carrier density occurs where n_{SQW} becomes greater than n_{CR} at certain onset temperatures, T_{ON1} and T_{ON2}, which depend on the excitation densities $P_1=200$ W/cm^2 and $P_2=95$ mW/cm^2, respectively. Since $T_{\mathrm{ON1}}<T_{\mathrm{ON2}}$, the model calculations demonstrate that an increased excitation results in a lower temperature at which equilibration occurs between the carrier densities for the CR and SQW regions. A further increase in temperature, independent of the excitation density, results in an inversion of the carrier density where n_{SQW} becomes greater than n_{CR}. Thus, the model nicely illustrates the influence of temperature and excitation on the steady-state carrier statistics for these coupled QW structures. For the structure of sample S1, the calculated values for $\Delta\phi_e$, $\Delta\phi_h$, n_{CR}, n_{SQW}, T_{ON1}, and T_{ON2} for varying temperatures and excitations exhibit a similar trend in comparison to the results for sample S2 in Fig. 9 and are, therefore, not shown.

Downloaded 11 May 2007 to 132.72.138.1. Redistribution subject to AIP license or copyright, see http://jap.aip.org/jap/copyright.jsp

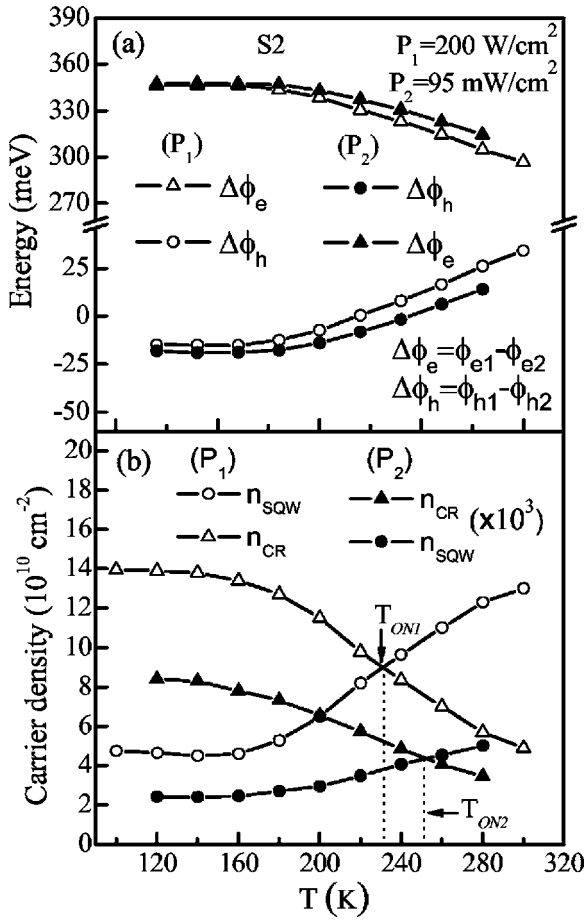

FIG. 9. The calculated differences in electron and hole quasi-Fermi levels between the CR and SQW regions, $\Delta\phi_e=\phi_{e1}-\phi_{e2}$ and $\Delta\phi_h=\phi_{h1}-\phi_{h2}$, vs temperature in (a) and the carrier densities in the CR and SQW regions (n_{CR} and n_{SQW}, respectively) vs temperature in (b). As the temperature increases, these calculations shown that $\Delta\phi_e$ and $\Delta\phi_h$ decrease in magnitude, indicative of an increased equilibration of the carrier densities between the CR and SQW regions.

IV. SUMMARY AND CONCLUSIONS

We have examined the carrier capture dynamics and excitation-dependent carrier statistics of coupled InGaN/GaN multiple quantum well samples. We measured the temporal evolution of time-delayed CL spectra to study the temperature and excitation-dependent transfer of carriers from a surrounding confinement region into a coupled single quantum well. Samples possessing two different structures for the confinement region (i.e., number of QWs and varying widths) were examined with CL. A sample possessing a single QW in the CR (sample S1) exhibited a more rapid transfer and collection of carriers into a coupled SQW in comparison to that for a sample possessing two QWs in the CR (sample S2). In order to study state filling of the SQW and QWs in the confinement region, we calculated the quasi-Fermi levels and carrier densities by utilizing a model that involves self-consistent solutions of the nonlinear Poisson-Schrödinger equation for wurtzite QWs including strain, deformation potentials, and polarizaion fields. Band-edge and effective mass parameters were first obtained from a strain- and In composition-dependent $\boldsymbol{k}\cdot\boldsymbol{p}$ calculation for wurtzite $In_xGa_{1-x}N$, using a 6×6 $\boldsymbol{k}\cdot\boldsymbol{p}$ Hamiltonian in the {0001} representation. The model shows that the difference in the quasi-Fermi levels between the confinement and SQW regions decreases with increasing excitation and temperature. Likewise, a reversal in the relative magnitude of the carrier densities between these two regions occurs at a certain temperature, which decreases as the excitation density is increased. Furthermore, the results for the model describing the steady-state excitation are consistent with those for transient excitation in time-resolved CL which also exhibit a marked increase in the rate of carrier transfer to the SQW region as the temperature increases. Thus, we show similar and important features in the temperature dependence of the carrier transfer between the coupled QWs of a surrounding confinement region and a target SQW for both transient excitation and steady-state excitations in the InGaN/GaN system.

ACKNOWLEDGMENT

This work was supported by the Israel Science Foundation (ISF Grant No. 8/02–1), the ARPA Optoelectronics Technology Center (OTC), the Office of Naval Research, and the Solid-State Lighting and Display Center.

[1] S. Nakamura, M. Senoh, S. Nagahama, N. Iwasa, T. Yamada, T. Matsushita, H. Kiyoku, and Y. Sigimoto, Appl. Phys. Lett. **68**, 2105 (1996); Jpn. J. Appl. Phys., Part 2 **35**, L74 (1996).
[2] S. Chichibu, T. Azuhata, T. Sota, and S. Nakamura, Appl. Phys. Lett. **70**, 2822 (1997).
[3] S. Chichibu, K. Wada, and S. Nakamura, Appl. Phys. Lett. **71**, 2346 (1997).
[4] Y. Narukawa, Y. Kawakami, M. Funato, S. Fujita, S. Fujita, and S. Nakamura, Appl. Phys. Lett. **70**, 981 (1997).
[5] T. Riemann, D. Rudloff, J. Christen, A. Krost, M. Lunenburger, H. Protzmann, and M. Heuken, Phys. Status Solidi B **216**, 301 (1999).
[6] X. Zhang, D. H. Rich, J. T. Kobayashi, N. P. Kobayashi, and P. D. Dapkus, Appl. Phys. Lett. **73**, 1430 (1998).
[7] J. Christen, T. Riemann, F. Bertram, D. Rudloff, P. Fischer, A. Kaschner, U. Haboeck, A. Hoffmann, and C. Thomsen, Phys. Status Solidi C **0**, 1795 (2003).
[8] H. Kollmer, J. S. Im, S. Heppel, J. Off, F. Scholz, and A. Hangleiter, Appl. Phys. Lett. **74**, 82 (1999).
[9] A. D. Bykhovski, V. V. Kaminski, M. S. Shur, Q. C. Chen, and M. A. Khan, Appl. Phys. Lett. **68**, 818 (1996).
[10] F. Bernardini, V. Fiorentini, and D. Vanderbilt, Phys. Rev. B **56**, R10024 (1997); Phys. Rev. Lett. **79**, 3958 (1997).
[11] A. Zoroddu, F. Bernardini, P. Ruggerone, and V. Fiorentini, Phys. Rev. B **64**, 045208 (2001).
[12] S. Chichibu, T. Azuhata, T. Sota, and S. Nakamura, Appl. Phys. Lett. **69**, 4188 (1996).
[13] J. Seo Im, H. Kollmer, J. Off, A. Sohmer, F. Scholz, and A. Hangleiter, Phys. Rev. B **57**, R9435 (1998).
[14] D. A. B. Miller, D. S. Chemla, T. C. Damen, A. C. Gossard, W. Wiegmann, T. H. Wood, and C. A. Burrus, Phys. Rev. Lett. **53**, 2173 (1984).
[15] P. Lefebvre, A. Morel, M. Gallart, T. Taliercio, J. Allegre, B. Gil, H. Mathieu, B. Damilano, N. Grandjean, and J. Massies, Appl. Phys. Lett. **78**, 1252 (2001).
[16] T. Deguchi, K. Sekiguchi, A. Nakamura, T. Sota, R. Matsuo, S. Chichibu, and S. Nakamura, Jpn. J. Appl. Phys., Part 2 **38**, L914 (1999).
[17] S. Keller, S. B. Fleischer, S. F. Chichibu, J. E. Bowers, U. K. Mishra, and S. P. DenBaars, Phys. Status Solidi B **216**, 269 (1999).
[18] H. T. Lin, D. H. Rich, A. Konkar, P. Chen, and A. Madhukar, J. Appl. Phys. **81**, 3186 (1997).
[19] U. Jahn, S. Dhar, O. Brandt, H. T. Grahn, and K. H. Ploog, J. Appl. Phys. **93**, 1048 (2003).
[20] S. Khatsevich, D. H. Rich, E.-T. Kim, and A. Madhukar, J. Appl. Phys. **97**, 123520 (2005).
[21] D. Bimberg, H. Munzel, A. Steckenborn, and J. Christen, Phys. Rev. B **31**, 7788 (1985).

Downloaded 11 May 2007 to 132.72.138.1. Redistribution subject to AIP license or copyright, see http://jap.aip.org/jap/copyright.jsp

[22]S. Khatsevich, D. H. Rich, S. Keller, and S. P. DenBaars, Phys. Rev. B **75**, 035324 (2007).
[23]P. Riblet, H. Hirayama, A. Kinoshita, A. Hirata, T. Sugano, and Y. Aoyagi, Appl. Phys. Lett. **75**, 2241 (1999).
[24]P. Lefebvre, S. Kalliakos, T. Bretagnon, P. Valvin, T. Taliercio, B. Gil, N. Grandjean, and J. Massies, Phys. Rev. B **69**, 035307 (2004).
[25]T. Kuroda and A. Tackeuchi, J. Appl. Phys. **92**, 3071 (2002).
[26]S. Kalliakos, P. Lefebvre, and T. Taliercio, Phys. Rev. B **67**, 205307 (2003).
[27]Y. D. Jho, J. S. Yahng, E. Oh, and D. S. Kim, Phys. Rev. B **66**, 035334 (2002).
[28]S. L. Chuang and C. S. Chang, Phys. Rev. B **54**, 2491 (1996); Semicond. Sci. Technol. **12**, 252 (1997).
[29]A. Bykhovski, B. Gelmont, and M. Shur, J. Appl. Phys. **74**, 6734 (1993).
[30]S. Khatsevich, D. H. Rich, X. Zhang, W. Zhou, and P. D. Dapkus, J. Appl. Phys. **95**, 1832 (2004).
[31]M. S. Minsky, S. B. Fleischer, A. C. Abare, J. E. Bowers, E. L. Hu, S. Keller, and S. P. Denbaars, Appl. Phys. Lett. **72**, 1066 (1998).
[32]A. Kunold and P. Pereyra, J. Appl. Phys. **93**, 5018 (2003).
[33]W. Shan, B. D. Little, J. J. Song, Z. C. Feng, M. Shurman, and R. A. Stall, Appl. Phys. Lett. **69**, 3315 (1996).
[34]A. V. Voznyy and V. G. Deibuk, Semiconductors **38**, 304 (2004).
[35]V. Fiorentini, F. Bernardini, F. D. Sala, A. D. Carlo, and P. Lugli, Phys. Rev. B **60**, 8849 (1999).
[36]F. Bernardini and V. Fiorentini, Phys. Status Solidi B **216**, 391 (1999).
[37]M. Leroux, N. Grandjean, J. Massies, B. Gil, P. Lefebvre, and P. Bigenwald, Phys. Rev. B **60**, 1496 (1999).
[38]U. M. E. Christmas, A. D. Andreev, and D. A. Faux, J. Appl. Phys. **98**, 073522 (2005).
[39]D. H. Rich, H. T. Lin, and A. Larsson, J. Appl. Phys. **77**, 6557 (1995).
[40]I.-H. Tan, G. L. Snider, L. D. Chang, and E. L. Hu, J. Appl. Phys. **68**, 4071 (1990).
[41]J.-W. Wu, Solid State Commun. **69**, 1057 (1989).
[42]P. Bigenwald, A. Kavokin, B. Gil, and P. Lefebvre, Phys. Rev. B **61**, 15621 (2000).

Downloaded 11 May 2007 to 132.72.138.1. Redistribution subject to AIP license or copyright, see http://jap.aip.org/jap/copyright.jsp